Differential Diagnosis of Lung Tumor with Positron Emission Tomography: A Prospective Study

Kazuo Kubota, Taiju Matsuzawa, Takehiko Fujiwara, Masatoshi Ito, Jun Hatazawa, Kiichi Ishiwata, Ren Iwata, and Tatsuo Ido

Department of Radiology and Nuclear Medicine, The Research Institute for Tuberculosis and Cancer, and Cyclotron Radioisotope Center, Tohoku University, Sendai, Japan

To predict the nature of non-calcifying lung tumors, we performed a prospective study of 46 cases with L-[methyl ^{11}C]methionine (MET, 24 cases) and ^{18}F-fluorodeoxyglucose (FDG, 22 cases) using positron emission tomography (PET). Mean tumor/muscle radioactivity ratios are 5.3 ± 2.0 (n = 14) for malignant and 1.9 ± 0.9 (n = 10) for benign with MET ($p < 0.001$), and 4.4 ± 2.2 (n = 12) and 1.5 ± 0.3 (n = 10), respectively, with FDG ($p < 0.001$). The ratios indicate that malignant tumors have higher metabolic demand than benign lesions. Tumors less than 1 cm in diameter were difficult to accurately evaluate due to PET resolution. Compared to the diagnosis at pathology, the MET study showed a sensitivity of 93% (13/14), a specificity of 60% (6/10), and an accuracy of 79% (19/24). The FDG study showed 83% (10/12), 90% (9/10), 86% (19/22), respectively. No significant differences were observed between the two tracers. This study suggests that PET studies using either MET or FDG may be very useful for the differential diagnosis of lung tumors.

J Nucl Med 1990; 31:1927–1933

Lung cancer is one of the major causes of death in many countries. The computed tomography (CT) scan has played an important role in diagnosis and staging of lung tumors (*1*), since CT can detect calcification, an important sign of a benign tumor. But if the tumor has soft-tissue attenuation without calcification, the differential diagnosis of cancer from a benign lesion is difficult (*2–4*). CT can provide excellent anatomic information but not metabolic or pathophysiologic information of the lesion.

The higher metabolic demands for glucose and amino acids in malignant tumors than normal tissues have been proven by both in vitro and in vivo experiments (*5–7*). Metabolic evaluation of cancer with positron emission tomography (PET) has been clinically demonstrated for brain tumor (*8*) and lung cancer using L-[methyl ^{11}C]-methionine (MET) (*9*) and ^{18}F-2-fluoro-2-deoxy-D-glucose (FDG) (*10*). However, the limited resolution of PET in some patients with small lesions and a known diagnosis of cancer makes it difficult to evaluate the differential diagnostic ability of PET. To determine the utility of PET in the differential diagnosis of lung tumors, we performed a prospective study of the differential diagnosis of lung tumor using MET and FDG.

MATERIALS AND METHODS

Patients

Forty-six patients (from 21 to 78 yr old, 15 women and 31 men) were examined with PET. They were referred to our hospital because of a tumor shadow in chest X-ray films with an unknown diagnosis. Maximum diameters of the tumors on CT ranged from 0.5 to 6.0 cm in the display for mediastinal setting (window-level 10 HW, window-width 300 HU). More than 60% (28/46) of the tumor diameters were 3 cm or smaller. No calcifications were seen in any tumors on CT. All patients were untreated primary cases for the PET study. CT was used to determine the image level of the greatest tumor diameter using identical positioning supports for both CT and PET. After the PET study, the pathologic diagnosis was obtained within 3 wk by operation (18 cases), needle biopsy (5 cases), transbronchial biopsy (21 cases) and sputum cytology (2 cases). Eight cases of nonmalignancy by transbronchial biopsy that responded to antibiotic treatment were clinically diagnosed as abscess. Follow-up of these cases for more than 1 yr confirmed the diagnosis of benignancy. The investigation was approved by the clinical research committee of our university and informed consent was obtained from every patient.

Radiopharmaceuticals

MET and FDG were synthesized using automated synthesis systems as described previously (*9,11,12*). Radiochemical purities were over 99%. Quality assurance tests for clinical use were performed according to the safety guidelines of our university. Tracers were randomly assigned to each patient. Twenty-four patients whose mean injection dose was 14.6 (2.0

Received Dec. 20, 1989; revision accepted May 10, 1990.

For reprints contact: Kazuo Kubota, MD, Department of Radiology and Nuclear Medicine, The Research Institute for Tuberculosis and Cancer, Tohoku University, 4-1 Seiryo-cho, Aoba-ku, Sendai 980, Japan.

- 36.0) mCi (540 MBq) were studied with MET. Twenty-two patients whose mean injection dose was 7.3 (3.5 - 13.0) mCi (270 MBq) were studied with FDG. The effect of variance on the injection doses has been evaluated previously (*9*); therefore, no significant correlation was observed between the injection dose and the tumor/muscle radioactivity ratio (T/M ratio), although the image quality and standard deviation of the region of interest (ROI) data were deteriorated in the small injection dose.

PET Scan

PT931/04 (CTI, Knoxville, TN) was used for 30 of the 46 patients. When it was out of service or was occupied by other patients, ECAT II (EG & G, Ortec, Oak Ridge, TN) was used for 16 patients. PT931/04 with four detector rings (512 BGO detectors/ring) provides seven-slice simultaneous acquisition with 7.15 mm width. The spatial resolution is 7.1 mm full width at half maximum (FWHM). ECAT II with single detector ring (66 NaI detectors/ring) provides single-slice acquisition with 18 mm width and a spatial resolution of 14 mm (FWHM). After the transmission scan using a 2-mCi germanium-68/gallium-68 ring source for the attenuation correction, MET or FDG was injected intravenously as a bolus. When the PT931/04 scanner was used, nine dynamic scans of 5 min each were performed over the seven slice levels, which totally covered a 5-cm width of the cross sections. To avoid partial volume effect in cases with small tumor, two 10-min interpolated scans were performed at 30 min postinjection. When the single-slice scanner ECAT II was used, three to five step-wise scans of 5 min each were performed at 30 min postinjection. The PET images were reconstructed using a measured attenuation correction and were corrected for decay.

Evaluation

Images obtained from 30 to 40 min after injection were considered to be the optimum with low blood-pool activity and constant activities of tumor and muscle in accordance with our previous studies (*9,13*), and, thus, were used for evaluation. About 80% of the radioactivity area of the tumor lesion, including the highest activity point, was used for the tumor ROI (mean tumor ROI size was 5.0 ± 1.9 cm^2). Then, to avoid the contamination of the non-tumor area, tumor ROIs were referred to both the transmission image and to the postinjection images, which showed the vascular structure. Dynamic data were not used for this study.

Six muscle ROIs were placed in the paravertebral, shoulder, and anterior chest muscle bilaterally in the same slice as the tumor. Muscle ROIs were placed on the transmission image first and then were copied to the corresponding emission

TABLE 1
Clinical, PET, and Histologic Findings in MET Study

Pt. no.	Age/Sex	Dose mCi	Dose MBq	Tumor size (cm)	T/M ratio	PET diag.	Histology	Method of diag.	Result
1	72/M	4.6	170	6.0 × 5.5	9.7	Malignant	Adeno	NB	T.P.
2	76/M	3.6	133	3.0 × 2.5	8.6	Malignant	Adeno	TB	T.P.
3	82/M	8.5	315	2.2 × 1.8	6.7	Malignant	Large cell	TB	T.P.
4	69/M	36.0	1332	2.0 × 1.5	6.0	Malignant	Squamous cell	NB	T.P.
5	60/M	10.7	396	5.0 × 4.5	5.8	Malignant	Large cell	TB	T.P.
6	61/F	18.0	666	5.5 × 4.0	5.5	Malignant	Small cell	TB	T.P.
7	62/M	13.5	500	3.5 × 2.5	5.3	Malignant	Squamous cell	TB	T.P.
8	39/M	9.0	333	5.0 × 4.0	5.2	Malignant	Adeno	TB	T.P.
9	69/M	18.4	681	3.0 × 3.0	5.0	Malignant	Large cell	TB	T.P.
10	78/M	6.0	222	1.0 × 1.0	4.4	Malignant	Squamous cell	Sp	T.P.
11	71/M	2.0	74	4.5 × 4.0	3.8	Malignant	Squamous cell	NB	T.P.
12	44/M	7.5	278	3.0 × 2.0	3.7	Malignant	Adeno	TB	T.P.
13	69/M	14.0	518	3.0 × 1.8	3.5	Malignant	Granuloma	TB + Cl	F.P.
14	46/M	12.0	444	5.4 × 4.0	3.0	Malignant	Abscess	TB + Cl	F.P.
15	45/F	32.0	1184	1.3 × 1.3	2.7	Malignant	Adeno	Op	T.P.
16	67/M	23.0	851	2.5 × 1.5	2.4	Malignant	Aspergilloma	Op	F.P.
17	62/M	8.3	307	0.8 × 0.8	2.2	Benign	Adeno	Op	F.N.
18	56/M	14.0	518	3.0 × 1.8	2.1	Malignant	Granuloma	Op	F.P.
19	59/M	24.0	888	5.0 × 4.0	2.1	Benign	Abscess	TB + Cl	T.N.
20	36/M	14.0	518	2.5 × 2.0	1.7	Benign	Abscess	TB + Cl	T.N.
21	66/F	13.0	481	1.5 × 1.0	1.3	Benign	Granuloma	TB + Cl	T.N.
22	63/F	31.0	1147	2.0 × 1.5	1.2	Benign	Granuloma	Op	T.N.
23	33/F	14.0	518	2.2 × 1.5	1.0	Benign	Hamartoma	Op	T.N.
24	21/M	14.8	548	5.0 × 2.5	0.9	Benign	Neurofibroma	NB	T.N.

Note: NB = needle biopsy; TB = transbronchial biopsy; Op = operation; Sp = sputum cytology; Cl = clinical course; T.P. = true-positive; T.N. = true-negative; F.P. = false-positive; F.N. = false-negative; and Dose = injection dose.

TABLE 2
Clinical, PET, and Histologic Findings in FDG Study

Pt. no.	Age/Sex	Dose mCi	Dose MBq	Tumor size (cm)	T/M ratio	PET diag.	Histology	Method of diag.	Result
1	60/M	5.8	215	5.0 × 4.0	8.2	Malignant	Large cell	TB	T.P.
2	51/M	7.0	259	5.0 × 4.5	6.3	Malignant	Adeno	Op	T.P.
3	72/M	6.9	255	4.0 × 3.0	6.0	Malignant	Squamous cell	TB	T.P.
4	58/F	10.7	396	1.5 × 1.5	5.8	Malignant	Adeno	Op	T.P.
5	56/F	6.3	233	6.0 × 5.0	5.4	Malignant	Squamous cell	Sp	T.P.
6	60/M	7.0	259	5.5 × 4.5	5.3	Malignant	Large cell	TB	T.P.
7	40/M	10.9	403	5.0 × 4.0	4.7	Malignant	Adeno	TB	T.P.
8	71/M	8.7	322	2.5 × 2.0	4.0	Malignant	Squamous cell	TB	T.P.
9	60/M	9.5	352	1.8 × 1.2	2.3	Malignant	Adeno	Op	T.P.
10	54/F	12.6	466	1.3 × 1.3	2.0	Malignant	Adeno	Op	T.P.
11	72/M	3.5	130	1.5 × 1.0	2.0	Malignant	Granuloma	TB + Cl	F.P.
12	50/M	3.7	137	4.5 × 3.0	2.0	Benign	Granuloma	Op	T.N.
13	46/M	7.0	259	2.5 × 2.0	1.8	Benign	Atelectasis	NB + Cl	T.N.
14	75/M	13.0	481	0.5 × 0.5	1.7	Benign	Squamous cell	Op	F.N.
15	35/M	10.2	377	3.0 × 2.0	1.7	Benign	Tuberculoma	Op	T.N.
16	53/M	7.0	259	4.0 × 1.5	1.5	Benign	Granuloma	Op	T.N.
17	61/F	7.4	274	2.0 × 1.0	1.5	Benign	Abscess	TB + Cl	T.N.
18	73/F	6.5	241	1.0 × 1.0	1.4	Benign	Hamartoma	Op	T.N.
19	47/F	8.3	307	1.5 × 1.0	1.2	Benign	Granuloma	Op	T.N.
20	65/F	3.1	115	2.0 × 1.5	1.1	Benign	Granuloma	TB + Cl	T.N.
21	39/F	4.5	167	3.5 × 2.2	1.1	Benign	Bronchogenic cyst	Op	T.N.
22	57/M	4.9	181	2.0 × 1.9	1.05	Benign	Liposarcoma	Op	F.N.

See Table 1 for definitions.

image with the same dimension in the display to minimize the partial volume effect. Mean pixel count of muscle area was obtained with averaging the four muscle ROIs, neglecting the maximum and minimum.

PET diagnosis of benignancy or malignancy was determined by using the T/M ratio or visual interpretation, according to our previous experience (*9,13–15*). After the PET study, the pathologic diagnosis was obtained and compared to the PET diagnosis, and sensitivity, specificity, accuracy were derived.

RESULTS

Detail of patients' data, tumor size on CT scan, final diagnosis of histopathology and its method, tracer dose, T/M ratio, and result of PET diagnosis are shown in Table 1 for the MET study and Table 2 for the FDG study. The distributions of the T/M ratios with MET were 5.3 ± 2.0 (n = 14) for malignant and 1.9 ± 0.9 (n = 10) for benign ($p < 0.001$), with a cut-off of 2.8. T/M ratios with FDG were 4.4 ± 2.2 (n = 12), 1.5 ± 0.3 (n = 10) ($p < 0.001$), and 2.0, respectively (Fig. 1). Most of the malignant tumors were clearly differentiated from the benign lesions using the T/M ratio both with MET and FDG. Some overlap, however, of the ratios on the border between malignancy and benignancy produced false diagnoses. The overlapping area of MET seemed to be wider than that of FDG.

Tumors less than 1 cm in diameter seemed to be too small for accurate evaluation. For tumors larger than 1 cm, the T/M ratios were separated into two groups of malignant and benign (Fig. 2), suggesting that the malignant tumors have higher metabolic demand than the benign tumors, independent of size.

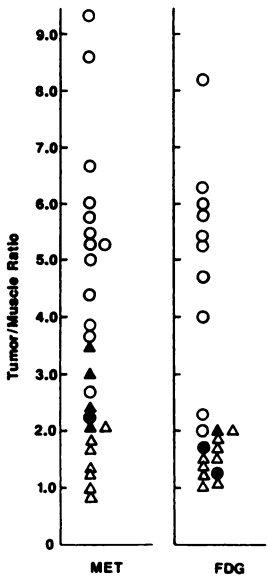

FIGURE 1
Distribution of T/M ratio with PET using FDG (right) and MET (left). Circles represent malignant pathology. Triangles represent benign pathology. Open symbols are true diagnosis and closed symbols are false diagnosis with PET.

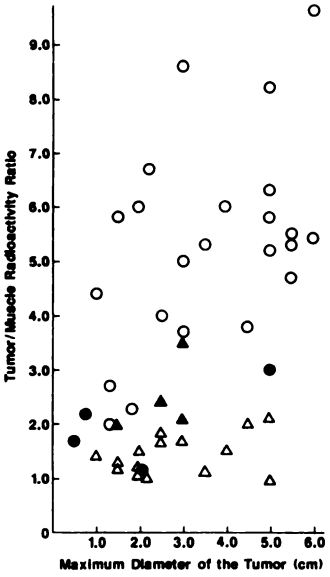

FIGURE 2
Distribution of T/M ratio with PET according to the tumor size. Both tracers FDG and MET are plotted together. Circles are malignant pathology and triangles benign pathology. Open symbols are true diagnosis with PET; closed are false diagnosis.

In the MET study, an adenocarcinoma (Case 17) of 0.8 cm in diameter was false-negative. Low T/M ratio can be explained by either the low count recovery due to the small size of the tumor or the tumor characteristics of low metabolic demand. Two granuloma (Cases 13 and 18), an aspergilloma (Case 16), and an abscess (Case 14) were false-positive. The other 19 cases were diagnosed correctly. A representative case of MET (Case 3) is shown in Figure 3.

In the FDG cases, a squamous cell carcinoma of 0.5 cm in diameter (Case 14) and a liposarcoma of fat deposition with a little cytoplasm (Case 22) were false-negative. A granuloma (Case 11) was false-positive. Other 19 cases were correctly diagnosed. A representative case of FDG (Case 8) is shown in Figure 4.

Table 3 presents the result of this prospective study. MET showed higher sensitivity, whereas FDG showed higher specificity. There are no significant differences by the Chi-square test. Overall sensitivity of both tracers is 88% (23/26); specificity, 75% (15/20); and accuracy, 83% (38/46). When the cases studied with PT931/04 were examined, the results were slightly improved in that the sensitivity of both tracers was 88% (14/16); specificity, 86% (12/14); and accuracy, 87% (26/30).

DISCUSSION

Clinical applications of FDG have been reported in metastatic liver tumor (*16*), brain tumor (*8*), and lung cancer (*10*). In the brain tumor study, pathologic grading of the glioma was correlated to the metabolic rate of glucose (*17*). In the head and neck tumors, the FDG uptake was correlated to the proliferative activity with the DNA flow cytometry (*18*). High FDG uptake of lung cancer was also reported (*10*) but neither correlation to the histopathology nor differentiation from the benign tumor has been studied.

The usefulness of MET uptake for the detection of cancer was reported through experimental (*19,20*) and clinical studies of lung cancer (*9,14,15*) and brain tumors (*21,22*). The correlation between the histopathologic type and the MET uptake has been observed in lung cancer (*13*). In this prospective study we evaluated both FDG and MET for differential diagnosis of unknown lung tumors.

Clinically, the respiratory movement appeared to affect tumor radioactivity. To avoid overcompensation of tumor radioactivities with uncertain count recovery

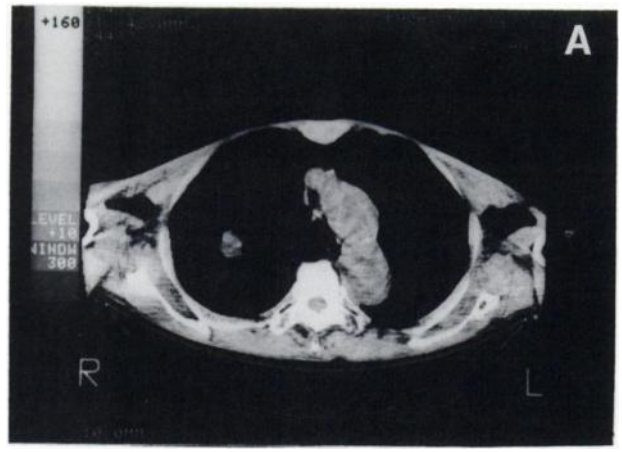

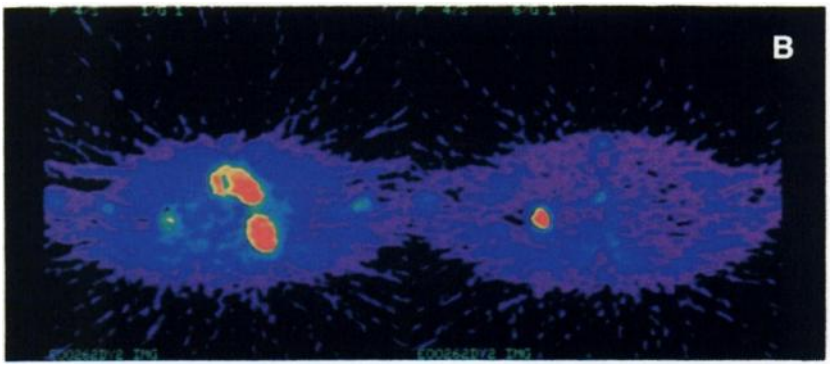

FIGURE 3
MET study of large cell carcinoma (Case 3). (A) CT scan showed a solitary pulmonary nodule in the right upper lobe. (B) Left: PET image 5 min after injection of 8.5 mCi (315 MBq) of MET showed high activity in the aorta and the superior vena cava but faint activity in the tumor. Right: PET image 35 min after injection showed very high activity in the tumor and low in the aorta.

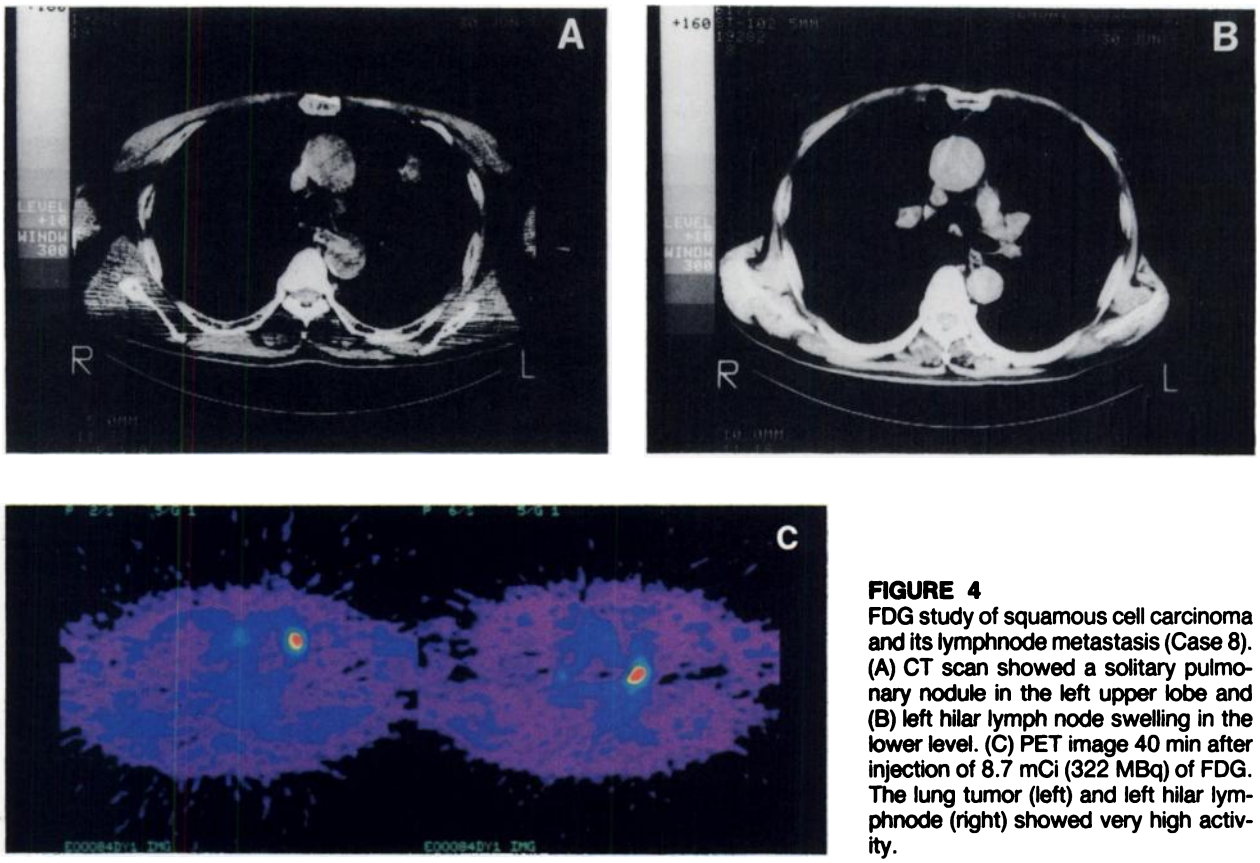

FIGURE 4
FDG study of squamous cell carcinoma and its lymphnode metastasis (Case 8). (A) CT scan showed a solitary pulmonary nodule in the left upper lobe and (B) left hilar lymph node swelling in the lower level. (C) PET image 40 min after injection of 8.7 mCi (322 MBq) of FDG. The lung tumor (left) and left hilar lymphnode (right) showed very high activity.

TABLE 3
Results of PET Studies for the Differential Diagnosis of Lung Tumor

MET Study of 24 Cases		
	Histologic diagnosis	
PET diagnosis	Malignant	Benign
Malignant	13	4
Benign	1	6
Total	14	10
Sensitivity	13/14 = 93%	
Specificity	6/10 = 60%	
Accuracy	19/24 = 79%	

FDG Study of 22 Cases		
	Histologic diagnosis	
PET diagnosis	Malignant	Benign
Malignant	10	1
Benign	2	9
Total	12	10
Sensitivity	10/12 = 83%	
Specificity	9/10 = 90%	
Accuracy	19/22 = 86%	

factors, we used a simple T/M ratio as an indicator of FDG or MET uptake. The constant radioactivity of FDG or MET in the muscle can be used as an internal standard (*9*). Although the T/M ratio is a simple and reliable indicator, tumors less than 1 cm in diameter seem to be difficult to accurately evaluate due to the PET resolution. Quantitative evaluation of MET uptake in tumor has been studied by us in different groups of patients using high-performance liquid chromatography analysis of plasma and the Patlak plot (*23,24*). Blood sampling and computation following the various models have improved the tumor metabolism data and have been helpful for diagnosis. In this study, blood sampling was not performed, however, the results showed that the T/M ratio seems to be satisfactory for clinical differential diagnosis.

In Figure 4, metastatic lymph adenopathy was clearly visualized. In some other cases, mediastinal or hilar lymph node was also observed. Some of the malignant tumors showed a borderline T/M ratio, which seems to be caused not by the low count recovery of the small size tumor but by the inherent characteristics of the tumor itself. Although glucose and amino acid metabolism are increased in most of the tumor, wide variation of glucose and amino acid consumptions, depending

on the type of neoplasm, is the current understanding of experimental tumor biochemistry. It seems to be the same in human lung cancers. The limitation of metabolic diagnosis with PET will exist in the heterogeneity of tumor metabolism while the metabolic demand itself induces the detection and grading of cancer with PET. A recent report showed high FDG uptake in abdominal abscess (*25*), which may be another limitation of differential diagnosis. Despite the aforementioned limitations, our study showed an accuracy of 83% for tumor diagnosis, possibly one of the most reliable among the noninvasive imaging techniques.

CONCLUSION

We found that the tracers FDG and MET showed no significant differences in sensitivity and specificity for the differential diagnosis of lung cancer. Most of the lung cancer cases were clearly differentiated from benign lesions using the T/M ratio with a high accuracy of 83%, suggesting that PET diagnosis of lung tumors is a useful clinical tool.

ACKNOWLEDGMENTS

This work was supported by Grant-in-Aid for Cancer Research from the Ministry of Health and Welfare (No. 1-40) and from the Ministry of Education, Science, and Culture (No. 01010025, 01570582). The authors thank Mr. Shoichi Watanuki and Mr. Shinya Seo for their PET operation and excellent technical assistances; Dr. Susumu Yamada and Ms. Roko Kubota for thoughtful advice; Mr. Yasuhiro Sugawara for photography; Miss Atsuko Yamamoto for illustrations; and the staff at the Cyclotron Radioisotope Center.

REFERENCES

1. Webb WR. Plain radiography and computed tomography in the staging of bronchogenic carcinoma: a practical approach. *J Thorac Imaging* 1987; 2:57–65.
2. Proto AV, Thomas SR. Pulmonary nodules studied by computed tomography. *Radiology* 1985; 156:149–153.
3. Siegelman SS, Khouri NF, Leo FP, Fishman EK, Braverman RM, Zerhouni EA. Solitary pulmonary nodules: CT assessment. *Radiology* 1986; 160:307–312.
4. Zerhouni EA, Stitik FP, Siegelman SS, et al. CT of the pulmonary nodule: a cooperative study. *Radiology* 1986; 160:319–327.
5. Warburg O. On the origin of cancer cells. *Science* 1956; 123:309–314.
6. Busch H, Davis JR, Honig GR, Anderson DC, Nair PV, Nyhan WL. The uptake of a variety of amino acids into nuclear proteins of tumors and other tissues. *Cancer Res* 1959; 19:1030–1039.
7. Isselbacher KJ. Increased uptake of amino acids and 2-deoxy-D-glucose by virus-transformed cells in culture. *Proc Natl Acad Sci USA* 1972; 69:585–589.
8. Di Chiro G, DeLaPaz RL, Brooks RA, et al. Glucose utilization of cerebral gliomas measured by [^{18}F]fluorodeoxyglucose and positron emission tomography. *Neurology* 1982; 32:1323–1329.
9. Kubota K, Matsuzawa T, Ito M, et al. Lung tumor imaging by positron emission tomography using C-11-L-methionine. *J Nucl Med* 1985; 26:37–42.
10. Nolop KB, Rhodes CG, Brudin LH, et al. Glucose utilization in vivo by human pulmonary neoplasms. *Cancer* 1987; 60:2682–2689.
11. Iwata R, Ido T, Saji H, et al. A remote-controlled synthesis of ^{11}C-iodomethane for the practical preparation of ^{11}C-labeled radiopharmaceuticals. *Int J Appl Radiat Isot* 1979; 30:194–196.
12. Iwata R, Ido T, Takahashi T, Monma M. Automated synthesis system for production of 2-deoxy-2-[^{18}F]fluoro-D-glucose with computer control. *Int J Appl Radiat Isot* 1984; 35:445–454.
13. Fujiwara T, Matsuzawa T, Kubota K, et al. Relationship between histologic type of primary lung cancer and carbon-11-L-methionine uptake with positron emission tomography. *J Nucl Med* 1989; 30:33–37.
14. Kubota K, Ito M, Fukuda H, et al. Cancer diagnosis with positron computed tomography and carbon-11-labeled L-methionine. *Lancet* 1983; 2:1192.
15. Kubota K, Matsuzawa T, Fujiwara T, et al. Differential diagnosis of solitary pulmonary nodules with positron emission tomography using [^{11}C]-L-methionine. *J Comput Assist Tomogr* 1988; 12:794–796.
16. Yonekura Y, Benua RS, Brill AB, et al. Increased accumulation of 2-deoxy-2-[^{18}F]fluoro-D-glucose in liver metastases from colon carcinoma. *J Nucl Med* 1982; 23:1133–1137.
17. DiChiro G. Positron emission tomography using [^{18}F]-fluorodeoxyglucose in brain tumors, a powerful diagnostic and prognostic tool. *Invest Radiol* 1987; 22:360–371.
18. Minn H, Joensuu H, Ahonen A, Klemi P. Fluorodeoxyglucose imaging: a method to assess the proliferative activity of human cancer in vivo. Comparison with DNA flow cytometry in head and neck tumors. *Cancer* 1988; 61:1776–1781.
19. Kubota K, Yamada K, Fukuda H, et al. Tumor detection with carbon-11-labeled amino acids. *Eur J Nucl Med* 1984; 9:136–140.
20. Kubota K, Matsuzawa T, Fujiwara T, et al. Differential diagnosis of AH109A tumor and inflammation by radioscintigraphy with L-[methyl-^{11}C]methionine. *Jpn J Cancer Res* 1989; 80:778–782.
21. Mosskin M, von Holst H, Bergström M, et al. Positron emission tomography with ^{11}C-methionine and computed tomography of intracranial tumours compared with histopathologic examination of multiple biopsies. *Acta Radiol* 1987; 28:673–681.
22. Von Schober O, Meyer G-J, Duden C, et al. Die Aufnahme von Aminosäuren in Hirntumoren mit der Positronen-Emissions-tomographie als Indikator für die Beurteilung von Stoffwechselaktivität und Malignität. *Fortschr Röntgenstr* 1987; 147:503–509.
23. Ishiwata K, Hatazawa J, Kubota K, et al. Metabolic fate of L-[methyl-^{11}C]methionine in human plasma. *Eur J Nucl Med* 1989; 15:665–669.
24. Hatazawa J, Ishiwata K, Ito M, et al. Quantitative evaluation of L-[methyl-^{11}C]methionine uptake in tumor using positron emission tomography. *J Nucl Med* 1989; 30:1809–1813.
25. Tahara T, Ichiya Y, Kuwabara Y, et al. High [^{18}F]-fluorodeoxyglucose uptake in abdominal abscesses: a PET study. *J Comput Assist Tomogr* 1989; 13:829–831.